Reaction chemistry and optimization of plasma remediation of N_xO_y from gas streams

Ann C. Gentile
University of Illinois, Department of Chemistry, 505 South Mathews, Urbana, Illinois 61801

Mark J. Kushner[a)]
University of Illinois, Department of Electrical and Computer Engineering, 1406 West Green Street, Urbana, Illinois 61801

(Received 22 August 1994; accepted for publication 10 April 1995)

Increasing environmental awareness and regulatory pressure have motivated investigations into energy efficient methods to remove oxides of nitrogen (N_xO_y) from gas streams resulting from the combustion of fossil fuels. Plasma remediation of N_xO_y is potentially an efficient removal technique due to the relative ease of generating reactants by electron-impact processes. Previous works have investigated the use of electron-beam, corona, and dielectric barrier discharge (DBD) generated plasmas for this purpose. In those works, reduction ($N+NO \rightarrow N_2+O$) and oxidation ($NO_2+OH \rightarrow HNO_3$) reactions were identified as major removal channels. A computational study of the plasma remediation of N_xO_y from humid air using repetitively pulsed DBDs is reported. The dominant reaction pathways are discussed and scaling laws are proposed to optimize the energy efficiency of removal. Three reaction periods are identified: the current pulse (during which electron-impact processes generate radicals), the postpulse remediative period (during which N_xO_y is removed), and the interpulse period (during which the densities of various nitrogen oxides are reapportioned with little net removal). The lifetimes of reactants (OH and O_3 in particular) determine the length of these periods and hence the optimum repetition frequency. Optimum repetition rates are typically less than hundreds of Hz. It is also found that a larger number of current pulses producing less energy deposition per pulse results in a higher removal efficiency due to reduced competition from radical-radical reactions which deplete the reactants. The production of unwanted species (e.g., O_3 and N_2O) can be minimized by reducing or terminating power deposition when the densities NO and NO_2 have been reduced to ppm levels. The energy efficiency of remediation generally increases with increasing water content by removing NO_x through the oxidation channel, although at the price of producing an acidic end product.

I. INTRODUCTION

Oxides of nitrogen (N_xO_y) in the atmosphere have been shown to be detrimental to human health and the environment.[1] As a result, the United States Environmental Protection Agency has established stringent limits on the allowable levels of N_xO_y emissions from the combustion of fossil fuels. For example, the allowable concentrations of N_xO_y (primarily NO and NO_2) in diesel exhaust in California will decrease to less than 50% of their present value in 1998. These developments have resulted in increasing economic and regulatory interest in developing energy efficient processes for the removal of N_xO_y from atmospheric pressure gas streams.

Various methods of plasma-based removal have been studied to efficiently remove N_xO_y from gas streams.[2] For example, electron-beam[3,4] and corona[5,6] generated plasmas have been investigated for remediation of SO_2/N_xO_y from coal-fired electrical power plants. Although high efficiencies have been demonstrated in these studies, plasma remediation of N_xO_y from mobile emission sources, such as diesel trucks, has more stringent requirements. The plasma sources must be lightweight, use low voltage, require minimum maintenance, and be easily scaleable as the rate of N_xO_y emission varies with vehicle speed and road conditions. The efficiencies required for these devices are also quite stringent. For example, consider a 100 hp diesel engine (flow rate 1 ℓ/s/hp) whose exhaust contains 500 ppm of NO. In order for the remediation process to consume less than 10% of the engine power, the maximum energy allowance is 51 eV/N_xO_y molecule removed. This efficiency must be realized without generating significant amounts of other unwanted species, such as N_2O or O_3.

Dielectric barrier discharges (DBD)[7] are compact, efficient plasma sources commonly used as ozonizers. DBDs are attractive for plasma remediation due to their ability to operate in a stable fashion at atmospheric pressures, with high average power and with low voltages (a few -10 kV) compared to coronas or electron beams. DBDs have previously been investigated for remediation of SO_2/N_xO_y resulting from the combustion of coal[8,9] and for remediation of volatile organic compounds[10,11] from atmospheric pressure gas streams. DBDs are composed of two parallel (or concentric) electrodes, at least one of which is covered by a dielectric. The gap in which the plasma is produced is typically 2–5 mm wide. An alternating voltage (hundreds of Hz to many kHz) is applied to the electrodes. When the applied voltage

a)Author to whom correspondence should be addressed; Electronic mail: mjk@uiuc.edu

 0021-8979/95/78(3)/2074/12/$6.00

exceeds the breakdown value, electron avalanches occur, resulting in a "forest" of microstreamers that function as conducting channels between the plates. Charge buildup on the dielectric during the current pulse reduces the net voltage across the gap. Eventually the electric field in the plasma is unable to sustain the microstreamer, and the plasma at that location is extinguished. Typically, the microstreamers are tens to hundreds of μm in diameter and 10s of ns in duration. The area density of the randomly distributed microstreamers (tens to many hundred/cm^2) is sufficiently large that on the average, the entire gas is processed.

The successful application of DBDs to plasma remediation of N_xO_y from mobile sources such as diesel exhaust will largely depend on the ability to meet the goals of obtaining high efficiency of remediation (low eV/molecule) and low production of undesirable compounds. In this article we discuss results from a modeling study of plasma remediation of N_xO_y from humid air. The purpose of this study is to elucidate the dominant reaction pathways and determine the discharge operating conditions which best meet the cited goals.

We discuss our computer model for the DBD and plasma chemistry in Sec. II. Section III is an overview of the remediation processes in which major reaction pathways and products are discussed. Results from a parametric study of plasma remediation of N_xO_y from humid air is presented in Sec. IV. Our concluding remarks are in Sec. V.

II. DESCRIPTION OF THE MODEL

We have developed a computer model for DBD processing of N_xO_y in which we have assumed uniform processing of the gas with each pulse. The structure of the model is described in Refs. 9 and 11 and so it is only briefly discussed here. The simulation consists of a circuit model, a solution of Boltzmann's equation for the electron energy distribution, and a plasma chemistry model. The circuit model provides *E/N* (electric field/gas number density) in the plasma which is used as input to the solution of Boltzmann's equation. Boltzmann's equation is solved using a two-term spherical harmonic expansion to determine the electron energy distributions from which electron-impact rate coefficients are generated. For the gas mixtures of interest ($N_2/O_2/H_2O/N_xO_y$) there are 42 electron-impact processes considered. The plasma chemistry model, containing 56 species and 331 reactions, uses the rate coefficients obtained from solving Boltzmann's equation along with temperature-dependent heavy particle reaction rate coefficients to produce species densities as a function of time. The plasma chemistry model also produces the plasma conductivity for use in the circuit model.

In the devices of interest, NO remediation is accomplished by a large number of discharge pulses each of which removes a small fraction of the total NO. We capture this behavior by running the model for a series of current pulses and afterglow periods, each lasting the inverse of the specified repetition rate. The initial conditions (species densities) of a given current pulse are provided by the densities obtained at the end of the afterglow of the previous current pulse. Although the DBD operates in a filamentary mode, the model presented here treats all quantities as volume averaged. We believe that the major scaling laws and reaction mechanisms are captured by this method. Exceptions to this these trends are discussed in Sec. IV.

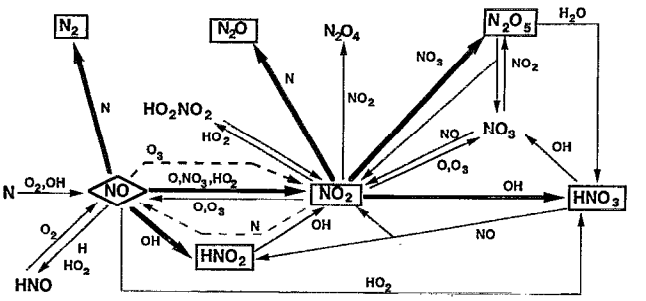

FIG. 1. Dominant reaction pathways, shown by arrows, for plasma remediation of N_xO_y. The initial toxin, NO, is shown by the diamond. The dominant end products are boxed. The radicals assisting in the reaction are noted adjacent to each arrow.

The electron-impact processes included in the model for $N_2/O_2/H_2O$ mixtures for atmospheric pressure discharges are discussed in Refs. 9 and 11. The important reactions included in the model for N_xO_y remediation are discussed in the following section. The efficiency of remediation is most sensitive to the rate of dissociation of N_2 by electron impact. Since this cross section is somewhat uncertain, we have performed a sensitivity analysis, whose results are also discussed in the following section.

III. REACTION MECHANISMS IN THE PLASMA REMEDIATION PROCESS

A. General characteristics

A schematic of the dominant reaction pathways for plasma remediation of N_xO_y is shown in Fig. 1. Reaction rate coefficients for these and other processes are listed in Table I. A complete listing of species and rate coefficients used in the model can be obtained by request from the authors. The initial toxin NO is highlighted by a diamond in Fig. 1. The six major end products, N_2, NO_2, N_2O, N_2O_5, HNO_2, and HNO_3, are boxed. Plasma remediation for operating conditions typical of DBDs progresses through radical assisted reactions and these radicals are listed next to the corresponding reaction arrow. There are two main remediation pathways for remediating NO:

$$\text{Reduction:}\quad NO+N\rightarrow N_2+O, \tag{1a}$$

and

$$\text{Oxidation:}\quad NO+O\rightarrow NO_2, \tag{1b}$$

$$NO_2+OH\rightarrow HNO_3. \tag{1c}$$

The preferred pathway depends on the desired end product. For stationary sources, the production of the acidic waste product may be acceptable since the acid can be readily collected and disposed of. For mobile sources, reduction is preferred over oxidation since the end products are N_2 and O. The former can be exhausted to the atmosphere. The latter generates radicals, primarily ozone, which can beneficial to the remediation process under certain circumstances. The

TABLE I. Dominant reactions in the plasma remediation of N_xO_y.[a]

Reaction	Rate coefficient[b]	Reference
$N+OH \rightarrow NO+H$	$3.8\times10^{-11}\exp(85/T)$	12
$N+O_2 \rightarrow NO+O$	$4.4\times10^{-12}\exp(-3220/T)$	12
$N+N+M \rightarrow N_2+M$	3.9×10^{-33}	13
$N+O+M \rightarrow NO+M$	$5.46\times10^{-33}\exp(155/T)$	14
$NO+H+M \rightarrow HNO+M$	3.4×10^{-32}	13
$NO+HO_2 \rightarrow HNO+O_2$	$9.10\times10^{-19}\exp(2819/T)$	15
$NO+HO_2+M \rightarrow HNO_3+M$	5.6×10^{-33}	c
$NO+HO_2 \rightarrow NO_2+OH$	$3.7\times10^{-12}\exp(240/T)$	12
$NO+N \rightarrow N_2+O$	3.1×10^{-11}	13
$NO+NO_3 \rightarrow NO_2+NO_2$	$1.6\times10^{-11}\exp(150/T)$	12
$NO+O+N_2 \rightarrow NO_2+N_2$	$9.1\times10^{-28}\,T^{-1.6}$	12
$NO+O_3 \rightarrow NO_2+O_2$	$2.00\times10^{-12}\exp(-1400/T)$	16
$NO+OH+M \rightarrow HNO_2+M$	$7.4\times10^{-31}\,(T/300)^{-2.4}$	12
$NO_2+HO_2+M \rightarrow HO_2NO_2+M$	$1.5\times10^{-31}\,(T/300)^{-3.2}$	12
$NO_2+N \rightarrow N_2O+O$	2.4×10^{-12}	13
$NO_2+N \rightarrow NO+NO$	6.0×10^{-13}	13
$NO_2+NO_2+M \rightarrow N_2O_4+M$	$1.4\times10^{-33}\,(T/300)^{-3.8}$	17
$NO_2+NO_3+M \rightarrow N_2O_5+M$	$2.7\times10^{-30}\,(T/300)^{-3.4}$	12
$NO_2+O \rightarrow NO+O_2$	$6.5\times10^{-12}\exp(120/T)$	12
$NO_2+O_3 \rightarrow NO+O_2+O_2$	1.0×10^{-18}	18
$NO_2+O+M \rightarrow NO_3+M$	$9.0\times10^{-32}\,(T/300)^{-2.0}$	12
$NO_2+O_3 \rightarrow NO_3+O_2$	$1.2\times10^{-13}\exp(-2450/T)$	12
$NO_2+OH+M \rightarrow HNO_3+M$	$2.2\times10^{-30}\,(T/300)^{-2.9}$	12
$N_2O_5 \rightarrow NO_3+NO_2$	2.8×10^{-2}	c
$N_2O_5+H_2O \rightarrow HNO_3+HNO_3$	5.0×10^{-21}	13
$HNO+O_2 \rightarrow NO+HO_2$	$5.25\times10^{-12}\exp(-1510/T)$	19
$HNO_2+OH \rightarrow NO_2+H_2O$	$1.8\times10^{-11}\exp(-390/T)$	12
$HNO_3+OH \rightarrow NO_3+H_2O$	$1.5\times10^{-14}\exp(650/T)$	20
$HNO_3+NO \rightarrow HNO_2+NO_2$	7.37×10^{-21}	21
$HO_2NO_2+M \rightarrow HO_2+NO_2+M$	$5.0\times10^{-6}\exp(-10\,000/T)$	12
$O(^1D)+H_2O \rightarrow OH+O$	2.2×10^{-10}	13
$O+O_2+M \rightarrow O_3+M$	$6.2\times10^{-34}\,(T/300)^{-2.0}$	12
$O+OH \rightarrow O_2+H$	$2.3\times10^{-11}\exp(110/T)$ cm^3 s^{-1}	22
$H+O_2+M \rightarrow HO_2+M$	4.8×10^{-32}	c,13
$H+OH+M \rightarrow H_2O+M$	8.6×10^{-31}	c

[a]A complete listing of reactions used in the model may be obtained by request from the authors.

[b]Rate coefficients have units of s^{-1} for one-body reactions, cm^3 s^{-1} for two-body reactions, and cm^6 s^{-1} for three-body reactions. Activation energies have equivalent units of K. T is the gas temperature. Two-body reactions that do not have specific temperature dependencies were scaled by $(T/300)^{1/2}$ to account for changes in the reaction rate due to thermal speeds. Three-body reactions were similarly scaled by $(T/300)^{-3/2}$.

[c]Rate coefficients were obtained from the evaluation of literature values in Ref. 23.

pathway which dominates is largely determined by the gas mixture and power deposition. Since, however, water is a product of the combustion process, it is difficult to completely eliminate the oxidation channel without drying the exhaust stream. This would be an energetically expensive procedure and impractical for mobile sources.

The predicted removal of NO in a DBD and the generation of the major end products are shown in Fig. 2 for an initial gas mixture of $N_2/O_2/H_2O=85/5/10$ at 400 K and 1 atm with a concentration of NO of 500 ppm. This gas mixture was chosen to capture the reduced oxygen and increased water content of combustion effluent. At the reference temperature and pressure, 1 ppm is equivalent to 1.83×10^{13} cm^{-3}. The DBD is pulsed at a repetition rate of 10 Hz with an energy deposition of 3 mJ/cm^3/pulse. The applied E/N (electric field/number density) has a peak value of 300 Td

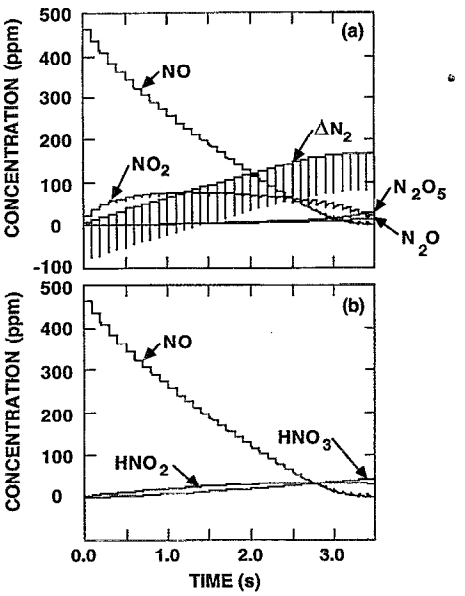

FIG. 2. Removal of NO and generation of end products in a DBD plasma remediation device: (a) NO, ΔN_2, and N_xO_y products; (b) NO and oxidation products HNO_2 and HNO_3. The initial gas mixture is $N_2/O_2/H_2O=85/5/10$ (1 atm, 400 K) with 500 ppm of NO. The repetition rate is 10 Hz and the energy deposition is 3 mJ/cm^3/pulse. The current pulse ($\approx$10 ns) cannot be resolved in this figure. The NO is primarily converted to N_2 and HNO_3.

(1 Td$=10^{-17}$ V cm^2). The duration of the current pulse, 10 ns, cannot be resolved in the figure. The short duration of the current pulse allows a high E/N to be sustained.[24]

The densities of NO, the incremental change in the density of N_2 [$\Delta N_2=N_2(t)-N_2(t=0)$], and the density of restricted N_xO_y products (NO_2,N_2O_5,N_2O) are shown in Fig. 2(a). ΔN_2 is an approximate measure of the amount of NO which is removed by the reduction channel since N_2 is a product of that process. The densities of NO and its oxidation products HNO_2 and HNO_3 are shown in Fig. 2(b). The majority of the removal of NO occurs rapidly compared to the interpulse period. The densities of the reaction products generally incrementally increase with each pulse as the products accumulate in the gas stream. An exception is the reaction product NO_2 which itself reacts with plasma generated radicals and is ultimately remediated. For these conditions, the total removal of NO (defined as achieving a density of <1 ppm) is obtained with a total energy deposition of 105 mJ/cm^3, or approximately 72 eV/molecule. NO is primarily converted to N_2 through the reduction channel (indicated by the increase in ΔN_2). Approximately 10% is converted to HNO_3 through the oxidation channel. Only a small amount (a few ppm) of the restricted oxides of nitrogen are formed.

The radicals which assist in the remediation are dominantly N, OH, O, H, HO_2, NO_3, and O_3. The primary radicals N, OH, and O are created by electron-impact reactions during the current pulse and are rapidly consumed by reactions in the remediation pathway. They are then regenerated during the next current pulse. This general behavior is shown in general in Fig. 3 for N and OH. There is some small pulse-to-pulse variation in the peak density of these species, but in general constant sources of N and OH are

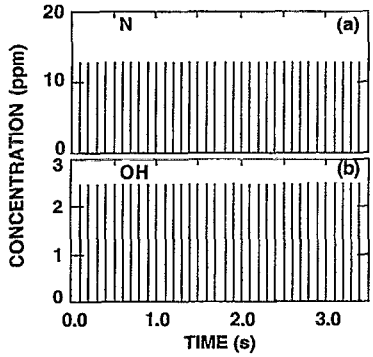

FIG. 3. Densities of (a) N and (b) OH radicals for the conditions of Fig. 2. These radicals are produced during the current pulse (not resolved in the figure) and are quickly consumed by the remediation reactions.

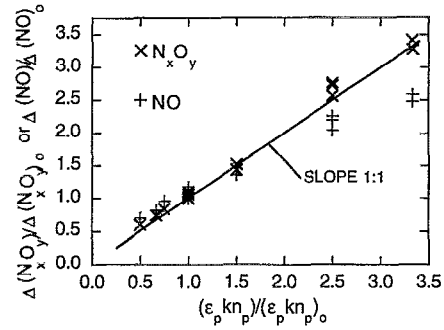

FIG. 4. Scaling relationship for remediation of N_xO_y. Removal of NO and N_xO_y are plotted as a function of $\beta=\epsilon_p k_d n_p$ (ϵ_p is the energy deposition/pulse, k_d the rate coefficient for electron-impact dissociation of N_2, and n_p the number of current pulses). Removal amounts and β are normalized by values obtained at $\epsilon_p=3$ mJ/cm^3, $k_d=9\times10^{-10}$ cm^3 s^{-1}, $n_p=3$. This scaling shows that for a large range of parameters, total removal of N_xO_y is nearly linearly proportional to β, with a small increase in efficiency at small ϵ_p.

produced by each current pulse. HO_2, NO_3, and O_3 are secondary radicals in that they are not formed by direct electron-impact events but rather by reactions involving the primary radicals. They are produced and consumed on longer time scales than the primary radicals and their densities are more sensitive to plasma conditions. The details of their behavior are discussed below.

B. Sensitivity of removal to the rate of dissociation of N_2

In gas mixtures having low water content (<20%), the dominant remediation pathway is the reduction reaction. The rate of dissociation of N_2 by electron impact is therefore of first-order importance with respect to the efficiency of remediation. The rate coefficient for dissociation of N_2 is obtained by convolving the electron energy distribution with the product of the electron-impact cross section and electron speed for all dissociative processes. In the discussion which follows, four separate dissociation cross sections were examined in this regard. The first three are measurements by Winters,[25] Zipf and McLaughlin,[26] and Cosby.[27] The fourth is a summation of electron-impact excitation cross sections to dissociative electronic states.[28]

The cross sections for dissociation of N_2 were used in solving Boltzmann's equations for the electron energy equation (EED), and the dissociation rate coefficient was compared at a reference E/N of 300 Td. Values for this rate coefficient varied from 2×10^{-10} to 9×10^{-10} cm^3 s^{-1}, with increasing variation at lower E/N. This variation is due in large part to uncertainties in the values of the cross sections near threshold (approximately 10 eV). Due to the "cutoff" nature of the EED in gas discharges, the slope of the cross section near threshold is more important than the peak or asymptotic values which are sampled in e-beam devices. Given the state uncertainties in the measurements near threshold (as large as 50%[27]), the rate coefficients for dissociation may have similarly large uncertainties.

As is discussed in the following section, for most of the conditions of interest the remediation of N_xO_y consists of a series of reactions which is initiated by the reduction reaction in Eq. (1a). One should expect, then, that the total removal of N_xO_y should be proportional to the total generation of N atoms by electron impact on N_2. To test this expectation, we performed a sensitivity analysis using as a scaling parameter $\beta=\epsilon_p k_d n_p$, where ϵ_p is the energy deposition/pulse, k_d is the rate coefficient for electron impact dissociation of N_2, and n_p is the number of discharge pulses. The total number of N atoms produced by electron-impact dissociation is proportional to β. As reference conditions we used $\epsilon_p=3$ mJ/cm^3, $k_d=9\times10^{-10}$ cm^3 s^{-1}, and $n_p=3$.

We varied these parameters over a large parameter space and compared the total removal of NO and N_xO_y normalized by their values at the reference conditions. The results are shown in Fig. 4. Over the range investigated, the total N_xO_y removed is nearly linearly proportional to β. There is, however, a tendency for more efficient removal when ϵ_p is smaller, and this scaling is discussed in Sec. IV. At large β, the amount of NO alone that is removed decreases due to the onset of nonlinear processes, which are also discussed in the following section. We also investigated the contributions of multistep dissociative excitation to removal of N_xO_y, and found that these processes contribute at most 10% to the total. These results imply that the calculated energy efficiency for N_xO_y removal will be inversely proportional to k_d. It is beyond the scope of this article to critically evaluate the available electron impact cross sections. We chose to use, then, the electron-impact dissociation cross section obtained from the summation of excitation to dissociative states. This yields a rate coefficient approximately 1.5 times that obtained using the cross sections of Zipf and McLaughlin,[25] and so can be considered a best case analysis. Since total removal of N_xO_y is linearly proportional to β, our cited efficiencies will be inversely proportional to k_d and so can be rescaled accordingly for a different choice of cross sections.

C. Detailed mechanisms

We now describe the reaction chemistry that occurs during remediation in more detail, by considering the chemistry that occurs during different time periods during and after the current pulse. The results of this analysis are then used in Sec. IV to help determine methods to optimize remediation.

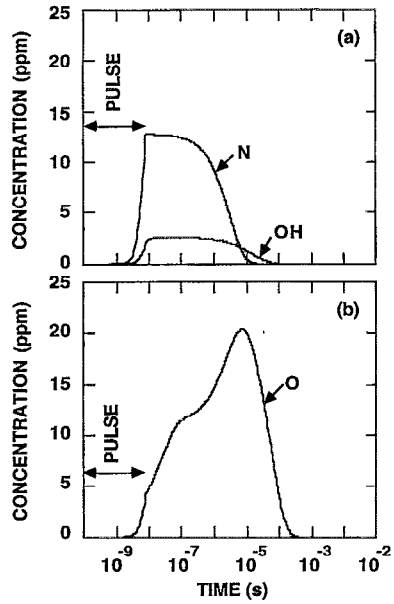

FIG. 5. Concentrations of primary radicals during and after a current pulse: (a) N and OH; and (b) O. The conditions are the same as for Fig. 2. The N and OH radicals are predominantly produced during the current pulse by electron impact processes. O is produced both during the current pulse by electron-impact reactions and after the current pulse by the reduction reaction $NO+N \rightarrow N_2+O$.

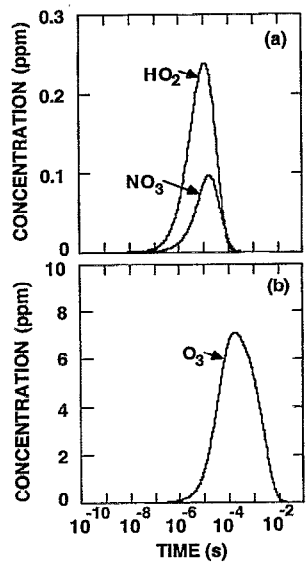

FIG. 6. Concentrations of secondary radicals which assist in the remediation of N_xO_y for the conditions of Fig. 1: (a) HO_2 and NO_3; and (b) O_3. The production of NO_3 and O_3 is dominantly by reaction of O atoms with NO_2 and O_2, respectively.

An individual current pulse and its subsequent intrapulse period can be characterized by three time scales, each making a different contribution to the total remediation. These three periods are: the current pulse having a duration of tens of ns, the postpulse remediative period (PPRP) spanning from tens of ns to hundreds of μs, and the interpulse period (IP), spanning from hundreds of μs to hundreds of ms or to the start of the next current pulse. The primary processes during the current pulse produce radicals by electron-impact collisions. During the PPRP, radical assisted remediation produces a net decrease in the concentration of N_xO_y molecules. During the IP, the total N_xO_y inventory does not significantly change, however, the apportioning between the various N_xO_y products does change.

During the current pulse, the primary radicals N, OH, O, and H are produced by electron-impact dissociation of the feedstock gases. N and OH, whose densities are shown in Fig. 5(a), have major direct roles in the remediation process through the reduction and oxidation channels. They are primarily produced by the reactions

$$e+N_2 \rightarrow N+N+e, \quad k=9\times10^{-10} \text{ cm}^3\text{ s}^{-1}, \tag{2}$$

$$e+H_2O \rightarrow H+OH+e, \quad k=6\times10^{-11} \text{ cm}^3\text{ s}^{-1}. \tag{3}$$

(The rate coefficients listed for electron-impact processes were obtained from our solution of Boltzmann's equation at $E/N=3\times10^{-15}$ V cm^2. See discussion in Sec. III B.) The densities of N and OH increase during the current pulse as a result of these reactions. Following the current pulse they monotonically decrease owing to their removal by remediation reactions and the lack of significant sources of N and OH in the absence of electron-impact processes. O atoms created during the current pulse are dominantly produced in their ground state, $O(^4S)$, and in the first excited state, $O(^1D)$,

$$e+O_2 \rightarrow O+O+e, \quad k=1\times10^{-9} \text{ cm}^3\text{ s}^{-1}, \tag{4a}$$

$$\rightarrow O+O(^1D)+e, \quad k=3\times10^{-9} \text{ cm}^3\text{ s}^{-1}. \tag{4b}$$

Reactions of $O(^1D)$ with water produce additional OH radicals,

$$O(^1D)+H_2O \rightarrow OH+OH, \tag{5}$$

however, the singlet state is not otherwise particularly important to the remediation process. Significant amounts of additional $O(^4S)$ are also produced during the PPRP by the reduction reaction for NO [Eq. (1a)] and to a lesser degree by reduction of NO_2,

$$NO_2+N \rightarrow N_2O+O. \tag{6}$$

These secondary sources of O atoms after the current pulse may exceed those by electron-impact collisions. This results in an increase in the density of O atoms early during the PPRP, as shown in Fig. 5(b). Ground-state O directly assists in the remediation process by oxidizing NO to NO_2, which is a necessary step in the oxidation channel. O, however, more importantly produces secondary radicals, O_3 in particular, which further assist in the remediation process. H atoms, produced by electron-impact processes [Eq. (3)], also generate secondary radicals (e.g., HO_2), but have no important direct contribution to remediation.

Secondary radicals HO_2, NO_3, and O_3, whose densities are shown in Fig. 6, also assist in the remediation. These radicals are formed by reactions involving the primary radicals H and O, and are necessarily produced on a longer time scale than the current pulse (tens of ns). For example, the

production of HO_2 and NO_3 peak at ≈ 10 μs, while that for O_3 peaks at ≈ 200 μs. The more significant of the reactions which produce secondary radicals are

$$H+O_2+M \rightarrow HO_2+M, \quad (7)$$

$$O+OH+M \rightarrow HO_2+M, \quad (8)$$

$$NO_2+O+M \rightarrow NO_3+M, \quad (9)$$

$$NO_2+O_3 \rightarrow NO_3+O_2, \quad (10)$$

$$O+O_2+N_2 \rightarrow O_3+N_2. \quad (11)$$

HO_2 is an intermediate in the oxidation of NO to NO_2. NO_3 also assists in the oxidation of NO, but more important oxidizes NO_2 to make the unwanted end product N_2O_5,

$$NO_2+NO_3 \rightarrow N_2O_5. \quad (12)$$

Note that the production of NO_3 will vary with the number of current pulses since the concentration of NO_2, its precursor reactant, depends on the number of current pulses as shown in Fig. 3(a).

Since radicals are responsible for remediation of N_xO_y, their lifetimes following the current pulse will determine the duration of such remediation. The primary radicals N and OH are largely responsible for total N_xO_y remediation (as opposed to reapportioning the various nitrogen oxides) and hence set its duration. The lifetime of O radicals is less tightly tied to the duration of remediation since the major role of O atoms is to produce secondary radicals. In addition to the direction remediation reactions and reactions which produce secondary radicals, the lifetimes of the primary radicals are also determined by the radical-radical reassociation reactions. The more important of these reactions are

$$N+N+M \rightarrow N_2+M, \quad (13)$$

$$N+O+M \rightarrow NO+M, \quad (14)$$

$$H+OH+M \rightarrow H_2O+M, \quad (15)$$

$$O+OH \rightarrow O_2+H. \quad (16)$$

The long time scale for remediation of solely NO is largely determined by the depletion time of the secondary radical O_3 as is discussed later in this subsection. The lifetime of N radicals, particularly when the density of NO is small, is also determined by

$$N+O_2 \rightarrow NO+O. \quad (17)$$

This reaction is important in determining the optimum power deposition for remediation, and is also discussed further below.

The details of the reaction chemistry and species densities during the PPRP and IP depend on the number of previous current pulses since the initial conditions for each pulse are determined by its previous history and by the accumulation of products. For this reason, we examine two pulses in detail: one early during the remediation of NO while the concentration of NO_2 is increasing (pulse 4 of Fig. 2), and one late during the remediation (pulse 17 of Fig. 2) when the density of NO_2 is decreasing. The concentrations of NO, N_xO_y, NO_2, and ΔN_2 for the early and late pulses are shown in Figs. 7 and 8, respectively. (In these and the following figures, densities labeled N_xO_y are the sum of the densities of all nitrogen oxides.)

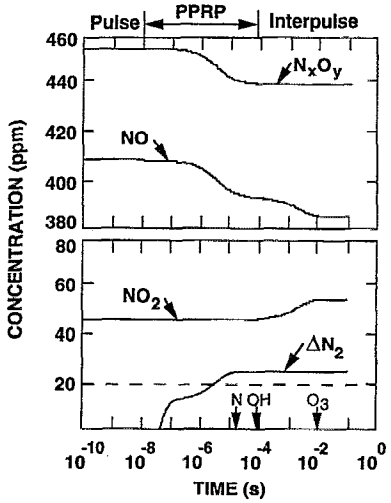

FIG. 7. Concentrations of NO, N_xO_y, NO_2, and ΔN_2 for the fourth pulse in Fig. 2. The durations of the current pulse, PPRP, and interpulse periods are shown at the top of the figure. The depletion times for the radicals N, OH, and O_3 which assist in the remediation are indicated on the axis. Although the density of NO decreases throughout the PPRP and IP, the total density of N_xO_y decreases only during the PPRP. During the IP, the inventory of N_xO_y is reapportioned among the various nitrogen oxides. In particular, the density of NO_2 increases.

In either case, remediation of NO and N_xO_y does not begin until after the end of the current pulse when a significant density of radicals has been produced. The densities of

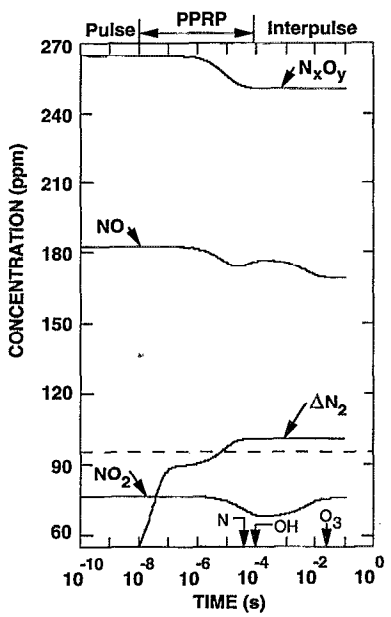

FIG. 8. Concentrations of NO, N_xO_y, NO_2, and ΔN_2 for the 17th pulse of Fig. 2. Depletion times for the radicals N, OH, and O_3 which assist in the remediation are indicated on the axis. The density of NO_2 decreases during the PPRP as a consequence of reduction reactions. Since the density of NO is less than in the earlier pulse, there is a larger supply of N atoms available for this process.

both NO and N_xO_y decrease during the PPRP due to conversion of NO and NO_2 to the following products:

$$NO \rightarrow N_2,\ HNO_2,\ NO_2, \tag{18a}$$

$$NO_2 \rightarrow HNO_3,\ N_2O,\ N_2O_5. \tag{18b}$$

These processes are also indicated by the bold solid arrows in Fig. 1. Remediation of N_xO_y and generation of these products continue until the assisting radicals (N, OH, and O_3) are depleted. The times at which N, OH, and O_3 are depleted are shown in Figs. 7 and 8. The depletion of N and OH correlates with the end of remediation of N_xO_y. The depletion of O_3 correlates with the end of remediation of NO. (Although O is longer lived than N and OH, its major role is generation of secondary radicals rather than direct assistance in the remediation.)

The density of ΔN_2 saturates when N is depleted. This signals the end of the reduction of NO. The majority of the remediation of N_xO_y has taken place by this time since reduction dominates over oxidation for these conditions. The end of the PPRP (for both the early and late pulses) occurs soon thereafter when the longer lived OH is depleted and the remediation of N_xO_y ceases. The density of NO, however, continues to decrease during the IP. This decrease results from NO being largely converted to NO_2 by O_3 by the reaction

$$NO + O_3 \rightarrow NO_2 + O_2 \tag{19}$$

(indicated by the bold dashed line in Fig. 1). This process continues until O_3 is depleted. The density of N_xO_y does not change during the IP in spite of the decrease in NO since the reaction with O_3 reapportions the densities of nitrogen oxides as opposed reducing the net density of nitrogen oxides.

The radicals which assist in the production of all major end products have depletion times occurring during the PPRP or slightly after its end. Therefore, the generation of products of NO remediation (N_2O, N_2O_5, HNO_2, and HNO_3) also largely occurs during the PPRP. The densities of these products, and the time at which the radical responsible for its generation is depleted, are shown in Fig. 9 for the early current pulse. The saturation of the product's density and depletion of the contributing radical are well correlated.

The behavior of the product NO_2 significantly varies between the two pulses. For the earlier pulse, NO_2 remains relatively constant during the PPRP as its creation and destruction processes balance. Its density increases during the IP, however, as a consequence of the reaction of NO with ozone [Eq. (19)]. This reaction accounts for approximately 1/3 of the removal of NO for the earlier pulse. The interpulse removal of NO and the production of NO_2 are therefore largely determined by the lifetime of O_3. It is important to reiterate that removal of NO by ozone during this period is misleading, as its removal produces NO_2 with no net reduction in the concentration of N_xO_y. This process does, however, prevent the buildup of O_3 which is itself a restricted species with respect to emission.

The change in behavior of NO_2 for the latter pulse (shown in Fig. 8) can be attributed to an additional major reaction during the PPRP. Following early pulses, N radicals

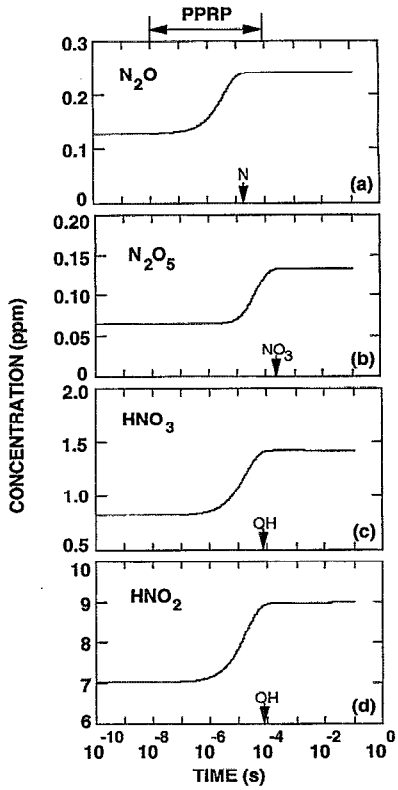

FIG. 9. Concentrations of major products of reduction and oxidation: (a) N_2O; (b) N_2O_5; (c) HNO_3; and (d) HNO_2. The generation of these products terminates when the assisting radicals are depleted. The time at which the assisting racial is depleted is indicated on that product's time axis.

were predominantly consumed by radical recombination and the reduction reaction in Eq. (1a). During later pulses, however, NO_2 also becomes a major reactant for the N radicals. This difference results from the increase in the density of NO_2 and the decrease in density of NO which would otherwise consume N atoms. The reaction of NO_2 with N (indicated by the plain dashed line in Fig. 1),

$$NO_2 + N \rightarrow NO + NO, \tag{20}$$

causes the density of NO_2 to decrease during the PPRP of the later pulse, as opposed to remaining relatively constant during the PPRP in the earlier pulse.

The reduction reaction of NO_2 in Eq. (20) replenishes NO, thus acting as a "back reaction" in the remediation scheme. The additional NO primarily enters the reduction channel. As a consequence, ΔN_2 is increased during the later pulse by reduction reactions not only with the NO present at the beginning of the pulse but also with the NO created by this back reaction. This is in contrast to the earlier pulse where the majority of ΔN_2 can be attributed to decreases in NO from its initial value for that pulse. The reaction sequence $NO_2 \xrightarrow{N} NO \xrightarrow{N} N_2$ [Eqs. (20) and (1a)] continues until N is depleted. At that time the concentration of NO briefly increases due to residual contributions from the back reaction [Eq. (20)] that can no longer be reduced due to the lack of N. Both NO and NO_2 then achieve quasisteady-state densities as the other PPRP reactions come to an end. As in the

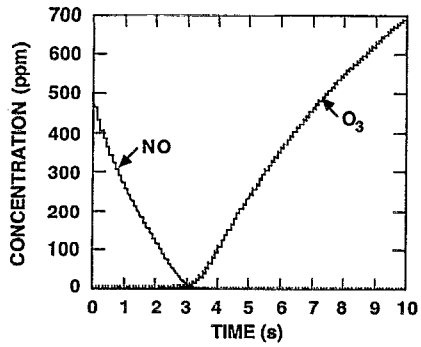

FIG. 10. Concentrations of NO and ozone for a sequence of current pulses exceeding that required to remediate the NO. The production of ozone increases after NO is depleted due to the elimination of its loss to reactions with NO.

earlier pulse, the dominant process during the IP exchanges NO for NO_2 [Eq. (19)]. Despite this additional source of NO_2 during the IP, there is a net decrease in the density of NO_2 during the later pulses due to the back reaction with N during the PPRP [Eq. (20)].

The reactions during the later pulse suggest that operation of the DBD after the depletion of NO can result in the buildup of restricted species. For example, once NO is depleted, the reaction in Eq. (19) (a major destruction mechanism for O_3) is no longer important. As a consequence, the density of O_3 increases on a pulse-to-pulse basis. This trend is shown in Fig. 10. Similarly, once NO and NO_2 are depleted, the reaction sequence $NO_2 \xrightarrow{N} NO \xrightarrow{N} N_2$ which consumes N atoms does not occur. At this juncture, N atoms serve as reactants which form additional N_xO_y [reactions initiated by Eq. (17)], rather than reducing NO_2 or NO. Concentrations of the major end products during remediation and at long times (many current pulses beyond that required to remove the initial NO) are shown in Fig. 11. At long times the concentrations of undesirable N_xO_y are tens to 100 ppm, and are comparable to the desired products, specifically ΔN_2 and HNO_3. The density of HNO_2 stops increasing after NO is depleted since its source ($NO+OH \rightarrow HNO_2$) is removed. Reactions with OH to produce NO_2 then deplete its density. The rate of production of HNO_3 decreases as the oxidation channel is slowed down due to the small amount of NO_2 which survives.

Due to the likelihood that restricted species will be produced in plasma remediation devices after the NO is depleted, a practical device should include an NO sensor that adjusts the DBD power level according to the concentration of NO in the exhaust. Power should be decreased or terminated to reduce or prevent the creation of the radicals O and N that lead to the formation of O_3 and N_xO_y as described above. Since the power deposition in a DBD can be varied from one cycle to the next, a feedback control loop is, in principal, straightforward.

Although ions do play important roles with regard to the characteristics of the plasma, they are not particularly chemically active with regard to N_xO_y remediation. The major ions consist of N_4^+, N_2O^+, N_2^+, O_2^+, H^-, O_2^-, NO_2^-, NO_3^-, and the cluster ions $H_3O^+H_2O$ and $H_3O^+(H_2O)_2$. The maximum

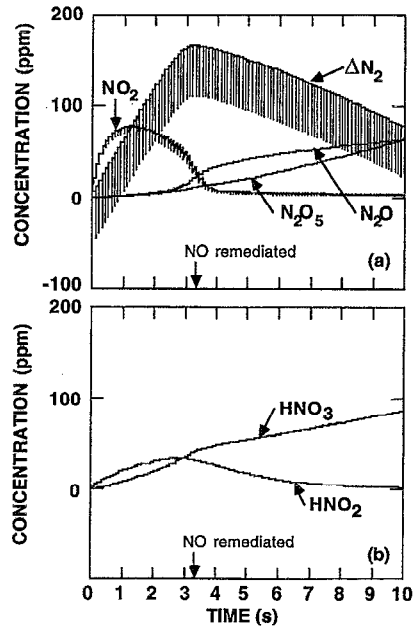

FIG. 11. Major end products for a sequence of current pulses exceeding that required to remediate NO: (a) ΔN_2 and N_xO_y products; (b) HNO_2 and HNO_3. After depletion of NO, N atoms which would otherwise be depleted by the reduction reaction with NO are available to produce other nitrogen oxides.

density of charged species is approximately 10^{13} cm^{-3}, with typical individual ions having maximum densities of 10^{11}–10^{12} cm^{-3}. Total ion, electron, representative positive, and representative negative ions are shown in Fig. 12 as a function of time for typical conditions. Positive (noncluster) ion densities are negligibly small at the onset of remediation after the current pulse. Such ions are chemically important only in that they may generate neutral radicals by dissociative recombination (e.g., $e+N_2^+ \rightarrow N+N$). However, even this contribution is small compared to the generation of radicals by direct electron-impact dissociation of the feedstock gases. In general, positive and negative ions react to form their corresponding neutral species, or in the case of the cluster ions, neutral water clusters or molecules. Since ion densities are small, these species are not created to any significant extent and so, again, do not contribute significantly to the remediation.

IV. OPTIMIZATION OF REMEDIATION CONDITIONS

Strategies for optimizing remediation of NO can be formulated in light of the chemical processes discussed in the prior section. We found that remediation is achieved primarily through neutral-radical-assisted reactions with ions playing a minor chemical role. Radicals are produced primarily during the current pulse (tens of ns) and are depleted by the remediation reactions. A multipulse format is thus required to replenish the radicals. We also found that a significant intrapulse time is required to take advantage of the radical-assisted remediation reactions. The optimum pulse repetition frequency is determined by the durations of these reactions (hundreds of μs to many ms) which are dictated by the radical lifetimes. Therefore, in deriving an optimal remediation

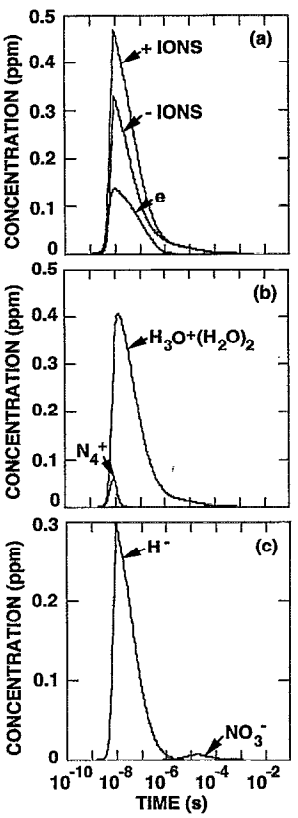

FIG. 12. Concentrations of selected charged particles. (a) Total positive ion, negative ion, and electron densities; (b) N_4^+ and cluster ion $H_3O^+(H_2O)_2$; (c) negative ion densities. The total charged species densities have peak values of $\approx 1\times10^{13}$ cm^{-3}.

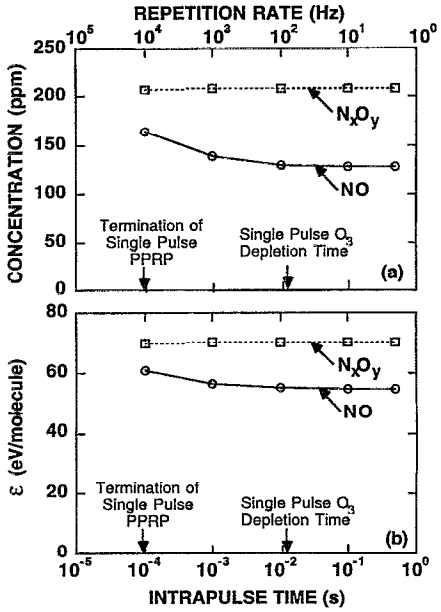

FIG. 13. Remediation parameters for NO and N_xO_y as a function of intrapulse time (or repetition rate): (a) concentration and (b) efficiency as a function of intrapulse time. The length of the PPRP for a single pulse and the O_3 depletion time are indicated on the time axis. N_xO_y remediation and efficiency are independent of intrapulse time for times greater than the PPRP. NO remediation and efficiency improve until O_3 is depleted.

strategy, it is important to consider the effects of parameters that affect radical formation, concentration, and lifetime, and that optimize radical usage.

To examine these dependencies we parameterized the model over interpulse time, energy deposition per pulse, applied voltage, and water content in the gas stream. To evaluate the efficiency of remediation, we define ϵ, which is energy deposition in eV/NO of N_xO_y molecule removed. Lower ϵ is more efficient. By defining ϵ in this manner we hope to capture the detrimental effects of merely converting NO to other nitrogen oxides, or producing additional nitrogen oxides. Although virtually total removal of NO can be achieved using DBDs, we consider the effect of these parameters on remediation at a total energy deposition of 60 mJ cm^{-3} as a point of comparison. Typically 20 pulses are required to achieve the desired 60 mJ cm^{-3}. In general, the conditions for each case are those of Sec. III with the exception of the parameter being varied.

Concentrations and remediation efficiencies of NO and N_xO_y are shown in Fig. 13 as a function of interpulse time or repetition rate. As might be anticipated from the single-pulse chemistry, N_xO_y remediation and efficiency are independent of the interpulse period for times longer than the PPRP which, for these conditions, is $\approx$100 μs (10^4 Hz). NO remediation and efficiency improve until O_3 is depleted, which for these conditions is $\approx$10 ms (10^2 Hz). Therefore, the net removal of N_xO_y is independent of repetition rate for practical devices (operating at less than many kHz). However, to minimize production of O_3, the repetition rate should be less than hundreds of Hz. The optimal interpulse time for both the removal of N_xO_y and minimizing the production of the undesirable end product O_3 is at least the O_3 depletion time of $\approx$1 ms.

The time scales for these processes can be varied by operating at different pressures. Although this is not a viable option for open remediation systems such as for diesel exhaust, it may be an option for closed-cycled industrial processes. In general, higher pressures produce shorter time scales since reactions occur more frequently with increasing reactant number. This change in time scales with pressure is shown in Fig. 14 where species densities for NO, N_xO_y, OH, and N_2O_5 are shown for operating at 1 and 1.7 atm. The density of OH is shown as a representative radical, and the density of N_2O_5 is shown as a representative end product. The onset and ending time of remediation, the radical formation and depletion times, and the onset and ending time of product formation all occur earlier for the higher pressure case. (Note that the absolute concentration values for these cases are misleading as the higher-pressure case has higher initial densities and therefore less energy deposited per molecule.) The shortened time scale for higher pressure will lead to a higher optimum repetition frequency.

Remediation and ϵ generally improve when using a larger number of current pulses delivering a smaller specific energy/pulse to achieve a desired total energy deposition, although this effect is not large over the parameter space of interest. This scaling is shown in Fig. 15. High specific power deposition produces a higher density of radicals and so one would expect more efficient remediation. However,

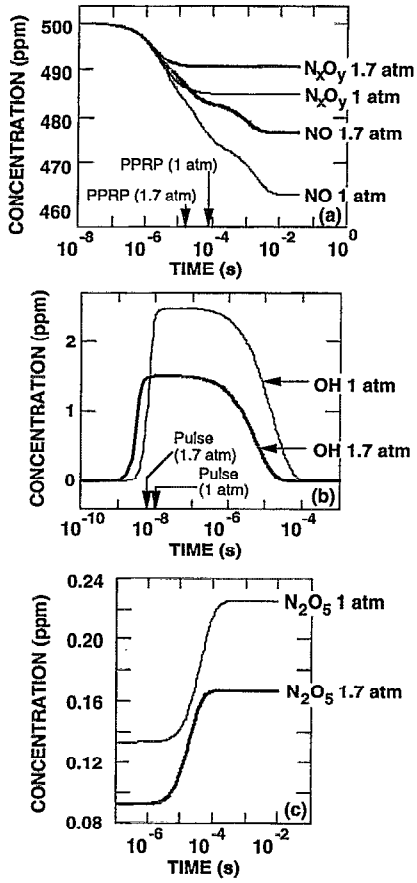

FIG. 14. Radical and product concentrations for operation at 1 and 1.7 atm as a function of time: (a) NO and N_xO_y; (b) OH; and (c) N_2O_5. The end of the current pulse and PPRP at each pressure are shown on the time axis. Reaction time scales generally decrease with increasing pressure.

the rates of the majority of remediation reactions scale linearly with radical concentration [e.g., Eq. (1)], while the rate of radical recombination reactions scale nonlinearly with radical concentration [e.g., Eq. (13)]. Therefore, lower specific power deposition results in fewer radical-radical reassociation reactions, and a more effective use of the radicals in direct remediation.

Our analysis, which uses spatially averaged quantities for a DBD (which actually occurs in filaments) captures the majority of the important scaling relationships. An exception is the just discussed scaling of the utilization of radicals as a function of average power deposition (energy deposition/pulse). Since power is deposited in microdischarges in an actual DBD, the local densities of primary radicals is larger for a given spatially averaged power deposition. Therefore, one should expect the efficiency of DBD remediation of N_xO_y to be a more sensitive function of average power deposition than cited here. From these scaling laws, the ideal DBD for N_xO_y remediation operates at moderate repetition rate (hundreds of Hz) with a large area density of microdischarges each having a low specific energy deposition.

For a given energy deposition, remediation and ϵ improve at higher applied E/N, as shown in Fig. 16. This scaling results from the fact that the fractional power deposition producing dissociation and ionization increases with increasing E/N relative to those processes which are nondissociative. This scaling is shown in Fig. 17 where the fractional power deposition by electron-impact processes is shown as a function of E/N. Power deposition is dominated by nondissociative electron-impact processes at $E/N<100$ Td. In the operating range of interest ($\approx$250–300 Td), the fraction of power deposition producing dissociation of N_2 is largest. In the quasisteady state, the operating E/N cannot, of course, be arbitrarily be chosen since its value will be determined by an

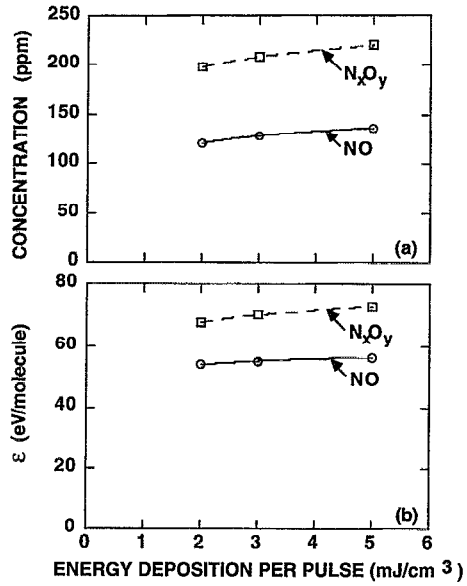

FIG. 15. Remediation parameters for NO and N_xO_y as a function of energy deposition/pulse: (a) concentration and (b) efficiency. Remediation improves using a larger number of current pulses delivering a smaller specific energy/pulse. At high specific energy deposition, radical-radical reactions compete with the remediation processes for reactants.

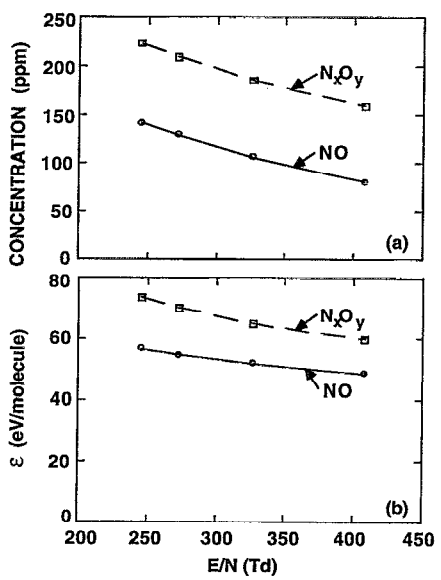

FIG. 16. Remediation parameters for NO and N_xO_y as a function of applied electric field: (a) concentration and (b) efficiency. N_xO_y remediation and efficiency improve with increasing E/N due to more efficient production of N atoms.

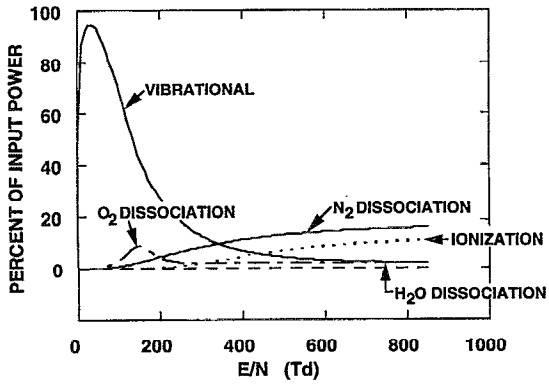

FIG. 17. Percent of input power dissipation by electron-impact processes as a function of applied electric field/number density E/N (1 Td=10^{-17} V cm^2). The fractional power deposition into dissociative and ionizing reactions increases with increasing E/N.

ionization balance. One does, however, have a greater degree of control over the bulk E/N when operating in the avalanche mode. This requires short pulse lengths which are on the order of the streamer transit time across the gap (5–10 ns).[24]

Significant improvement in remediation and ϵ can also be obtained with increasing water content in the gas stream, as shown in Fig. 18. This trend is due to the increased removal of NO and NO_2 by oxidation. The large range for the efficiencies obtained while varying the water content indicates that the availability of the oxidation channel is a major leverage in remediation.

V. CONCLUDING REMARKS

Dielectric barrier discharges are potentially an effective technology for the remediation of N_xO_y. NO can be removed from atmospheric gas streams from concentrations of 500 to <1 ppm with an energy expenditure of <70–105 eV/molecule. For typical diesel engines, this efficiency corresponds to as low as 15% of the engine power output. Remediation of NO to concentrations below statutory amounts (<100 ppm) requires energy expenditures of <60–90 eV/molecule. Uncertainties in the ranges of these energy expenditures are largely due to uncertainties in the rate of dissociation of N_2 in the discharges of interest. The end products of the remediation are primarily N_2 and HNO_3. Only small amounts of restricted nitrogen oxides or ozone are formed as long as the device is not operated at power levels beyond that required for total NO remediation. The optimal interpulse time for remediation is at least as long as the O_3 depletion time. In closed-cycle systems these time scales can be varied to fit constraints on repetition rate by adjusting the total gas pressure. Removal efficiency is higher when using more current pulses of lower energy, larger applied voltage, and larger H_2O percentage in the gas stream. Our results indicate that even for mobile applications, it may be worthwhile to take advantage of the oxidation pathway which leads to the acidic waste product because of the significantly improved efficiency.

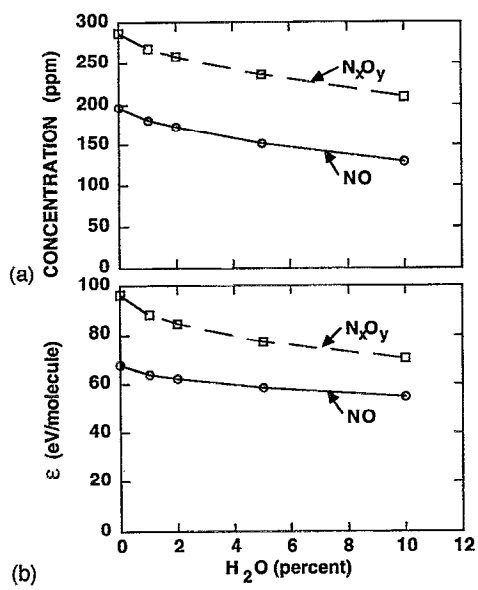

FIG. 18. Remediation parameters for NO and N_xO_y as a function of water content in the gas stream: (a) concentration and (b) efficiency. N_xO_y remediation and efficiency improve with increasing H_2O percentage due to the larger contribution of the oxidation channel.

ACKNOWLEDGMENTS

This work was supported by the National Science Foundation (Grants No. CTS 94-12565 and No. ECS 91-09326) and the Office of Naval Research (Contract No. N00014-94-1-0819).

[1] J. D. Splenger, M. Brauer, and P. Koutrakis, Environ. Sci. Technol. **24**, 946 (1990).
[2] A collection of articles on various plasma technologies being investigated for plasma remediation of toxic gases appears in *Non-Thermal Plasma Techniques for Pollution Control—Part A: Overview, Fundamentals and Supporting Technologies*, edited by B. Penetrante and S. Schulthesis (Springer, New York, 1993); *Non-Thermal Plasma Techniques for Pollution Control—Part B: Electron Beam and Electrical Discharge Processing*, edited by B. Penetrante and S. Schulthesis (Springer, New York, 1993).
[3] D. J. Helfritch, in *Non-Thermal Plasma Techniques for Pollution Control—Part B: Electron Beam and Electrical Discharge Processing*, edited by B. Penetrante and S. Schulthesis (Springer, New York, 1993), pp. 33–46.
[4] I. Gallinberti, Pure Appl. Chem. **60**, 663 (1988).
[5] S. Masuda, Pure Appl. Chem. **60**, 727 (1988).
[6] K. Kawamura and V. H. Sui, Radiat. Phys. Chem. **24**, 117 (1984).
[7] B. Eliasson, M. Hirth, and U. Kogelschatz, J. Phys. D **20**, 1421 (1987); B. Eliasson and U. Kogelschatz, Appl. Phys. B **46**, 299 (1988).
[8] S. K. Dhali and I. Sardia, J. Appl. Phys. **69**, 6319 (1991).
[9] M. B. Chang, J. H. Balbach, M. J. Rood, and M. J. Kushner, J. Appl. Phys. **69**, 4409 (1991).
[10] L. A. Rosocha, G. K. Anderson, L. A. Bechtold, J. J. Coogan, H. G. Heck, M. Kang, W. H. McCulla, R. A. Tennant, and P. J. Wantuck, in *Non-Thermal Plasma Techniques for Pollution Control—Part B: Electron Beam and Electrical Discharge Processing*, edited by B. Penetrante and S. Schulthesis (Springer, New York, 1993), pp. 281–308.
[11] D. Evans, L. A. Rosocha, G. K. Anderson, J. J. Coogan, and M. J. Kushner, J. Appl. Phys. **74**, 5378 (1993).
[12] R. Atkinson, D. L. Baulch, R. A. Cox, R. F. Hampson, Jr., J. A. Kerr, and J. Troe, J. Phys. Chem. Ref. Data **18**, 881 (1989).
[13] J. C. Person and D. O. Ham, Radiat. Phys. Chem. **31**, 1 (1988).
[14] I. M. Campbell and C. N. Gray, Chem. Phys. Lett. **18**, 607 (1973).
[15] C. J. Howard, J. Chem. Phys. **71**, 2352 (1979).
[16] W. B. DeMore, D. M. Golden, R. F. Hampson, C. J. Howard, M. J.

Kurylo, M. J. Molina, A. R. Ravishankara, and S. P. Sander, JPL **87-41**, 1 (1987).
[17] P. Borrell, C. J. Cobos, and K. Luther, J. Phys. Chem. **92**, 4377 (1988).
[18] J. Hjorth, J. Notholt, and G. Restelli, Int. J. Chem. Kin. **24**, 51 (1992).
[19] N. Fujii, H. Miyama, M. Koshi, and T. Asuba, Symp. (Int.) Combust. Proc. **18**, 873 (1981).
[20] S. Mukkavilli, C. K. Lee, K. Varghese, and L. L. Tavlarides, IEEE Trans. Plasma Sci. **PS-16**, 652 (1988).
[21] R. Svensson and E. Ljungström, Int. J. Chem. Kin. **20**, 857 (1988).
[22] W. Tsang and R. F. Hampson, J. Phys. Chem. Ref. Data **15**, 1087 (1986).
[23] W. G. Mallard, F. Westley, J. T. Herron, R. F. Hampson, and H. H. Frizzell, NIST Chemical Kinetics Database Ver. 5.0, NIST Standard Reference Data, Gaithersburg, MD, 1993.
[24] P. A. Vitello, B. M. Penetrante, and J. N. Bardsley, Phys. Rev. E **49**, 5575 (1994).
[25] H. F. Winters, J. Chem. Phys. **44**, 1472 (1966).
[26] E. C. Zipf and R. W. McLaughlin, Planet. Space Sci. **26**, 449 (1978).
[27] P. C. Cosby, J. Chem. Phys. **98**, 9544 (1993).
[28] Y. Itikawa, M. Hayashi, A. Ichimura, K. Onda, K. Sakimota, and K. Takayanagi, J. Phys. Chem. Ref. Data **15**, 985 (1986).